Seismic performance analysis of steel-brace RC frame using topology optimization

Shengfang Qiao[*1,2], Huqing Liang[3], Mengxiong Tang[1], Wanying Wang[4] and Hesong Hu[1]

[1]Guangzhou Institute of Building Science Co., Ltd., Baiyun, Guangzhou 510440, China
[2]School of Civil Engineering and Transportation, South China University of Technology, Tianhe, Guangzhou 510641, China
[3]Guangzhou Municipal Construction Group Co., Ltd., Yuexiu, Guangzhou 510030, China
[4]School of Civil Engineering and Transportation, Guangdong University of Technology, Panyu, Guangzhou, 510006, China

Abstract. Seismic performance analysis of steel-brace reinforced concrete (RC) frame using topology optimization in highly seismic region was discussed in this research. Topology optimization based on truss-like material model was used, which was to minimum volume in full-stress method. Optimized bracing systems of low-rise, mid-rise and high-rise RC frames were established, and optimized bracing systems of substructure were also gained under different constraint conditions. Thereafter, different structure models based on optimized bracing systems were proposed and applied. Last, structural strength, structural stiffness, structural ductility, collapse resistant capacity, collapse probability and demolition probability were studied. Moreover, the brace buckling was discussed. The results show that bracing system of RC frame could be derived using topology optimization, and bracing system based on truss-like model could help to resolve numerical instabilities. Bracing system of topology optimization was more effective to enhance structural stiffness and strength, especially in mid-rise and high-rise frames. Moreover, bracing system of topology optimization contributes to increase collapse resistant capacity, as well as reduces collapse probability and accumulated demolition probability. However, brace buckling might weaken beneficial effects.

Keywords: topology optimization; collapse resistant capacity; steel brace; seismic performance assessment; incremental dynamic analysis; residual deformation

1. Introduction

Adding steel brace was profitable to enhance seismic performance of RC frame in highly seismic region. Ozcelik *et al.* (2012) studied the seismic performance of RC frame with steel brace. Different steel brace configurations were compared by Akbari *et al.* (2015). Della *et al.* (2015) used buckling restrained brace to repair damaged RC frame. Seismic performance of steel-brace RC frame has been highlighted in previous researches. However, reasonable bracing systems in RC frame were still not well concerned.

Actually, topology optimization was very useful to found reasonable structure configuration in building structure. Allahdadian and Boroomand (2016) introduced a topology optimization configuration considering earthquake records using SIMP method. Zhang *et al.* (2016) discussed optimized configurations based on ground structure method by deleting elements. In order to study the available bracing configuration, Suksuwan and Spence (2018) discussed lateral configuration in high-rise buildings. Tangaramvong and Tin-Loi (2015), Zhu *et al.* (2017) derived optimal configuration of steel frame using ground structure method. Numerical instabilities, e.g. unshaped boundary and checkerboard phenomenon in topology optimization, were found sometimes due to removing elements in the researches mentioned above. Topology optimization based on truss-like material model was introduced in Qiao and Zhou (2016), and numerical instabilities were settled. Qiao *et al.* (2016) discussed bracing configuration in steel frame based on truss-like material model. In addition, conceptual configurations of high-rise steel braced frame under multiple loading cases (including wind and earthquake) were presented in Qiao *et al.* (2017), and it was indicated that seismic performance of high-rise steel braced frame based on topology optimization could be improved.

Topology optimization has been widely used in steel frame for now. However, bracing configuration of RC frame in highly seismic region was rarely studied. Generally, structural characteristics between steel frame and RC frame were markedly different, especially in seismic performance. Collapse resistant capacity of RC frame was worse than steel frame, and RC frame could be more prone to be demolished due to severe damage in Ramirez and Miranda (2012). However, reasonable bracing systems in RC frame were still not well considered in highly seismic region. Comprehensive seismic performance analysis of steel-brace RC frame based on topology optimization was hardly discussed. Therefore, it was not sure if topology optimization was beneficial to steel-brace RC frame in highly seismic region.

On the basis of previous studies, bracing system of steel-brace RC frame using topology optimization (or TPB)

∗Corresponding author, Ph.D.
 E-mail: sfqiao@yahoo.com

based on truss-like material model was studied in highly seismic region. Seismic action was predominant in RC frame of highly seismic region. Therefore, topology optimization based on truss-like material model under seismic action was presented. TPB was used in different RC frame. Moreover, comprehensive seismic performance analysis of RC frame with different bracing system was discussed and compared in this study.

2. Seismic performance analysis of steel-brace RC frame using topology optimization

2.1 Optimized bracing system using truss-like material model

2.1.1 Truss-like material model under minor earthquake

Finite element mesh was used to divide initial domain in Fig. 1(a), and the initial domain was strengthened by truss-like material. The truss-like members in Fig. 1(b) were demonstrated at nodes, and the interpolation method was used to obtain members distribution inside the elements. t_{1j} and t_{2j} in Fig. 1(c) denote the densities of orthogonal members at node "j", as well as a_j and $a_{j+\pi/2}$ represent the directions accordingly. Further, the stiffness matrix each element "e" can be obtained.

$$k_e = \int_{V_e} \boldsymbol{B}^T \boldsymbol{DB} \mathrm{d}V = \sum_{j \in S_e} \sum_b t_{bj} \sum_r g_r(\alpha_j) \boldsymbol{H}_{ejr} \quad (1)$$

Qiao and Zhou (2016), Qiao *et al.* (2016) introduced the truss-like material model in detail. Therefore, the detailed derivation process was not presented herein. r=1, 2, 3 and b=1, 2 in Eq. (1).

$$\boldsymbol{H}_{ejr} = E \int_{V_e} N_j \boldsymbol{B}^T \boldsymbol{A}_r \boldsymbol{B} \mathrm{d}V$$

and g_r was element of matrix [cos2α sin2α 1].

Initial global stiffness matrix $\boldsymbol{K}$ was derived.

$$\boldsymbol{K} = \sum_e \boldsymbol{k}_e \quad (2)$$

Finite element equation was obtained as follows.

$$\boldsymbol{KU} = \boldsymbol{F} \quad (3)$$

Where $\boldsymbol{F}$ was force vector and $\boldsymbol{U}$ was displacement vector. Stress matrix σ can be gained.

$$\sigma = \boldsymbol{DBU} = \boldsymbol{DBK}^{-1}\boldsymbol{F} \quad (4)$$

Further, stress matrix of node "j" was presented.

$$\sigma_j = [\sigma_{xj} \quad \sigma_{yj} \quad \tau_{xyj}] \quad (5)$$

Where σ_{xj} or σ_{yj} was normal stress, and τ_{xyj} was shear stress. Angle of principal stress α_j and relevant principal stress were solved.

$$\alpha_j = \frac{1}{2}\arctan\frac{\tau_{xyj}}{\sigma_{xj} - \sigma_{yj}} \quad (6)$$

$$\sigma_{1j,2j} = \frac{\sigma_{xj} + \sigma_{yj}}{2} \pm \sqrt{(\frac{\sigma_{xj} - \sigma_{yj}}{2})^2 + \frac{\tau_{xyj}^2}{4}} \quad (7)$$

2.1.2 Topology optimization model with minimum volume

Topology optimization model with minimum volume under minor earthquake was introduced.

$$\begin{aligned} &\text{find} \quad \alpha_j, t_{bj} \geq \underline{t} \quad b = 1,2 \\ &\text{min} \quad \sum_e V_e \quad j = 1,2,...,n \\ &\text{s.t.} \quad \sigma_{bj} \leq \sigma_y \end{aligned} \quad (8)$$

where V_e was material volume of element "e", and σ_y was yielding stress. In order to minimize material volume in Eq. (8), σ_{bj} was yield stress at each node in full-stress method. Two truss-like members were distributed at relevant principal stress directions and updated after iteration. Therefore,

$$t_{bj}^{i+1} = t_{bj}^i \sigma_{bj}^i / \sigma_y, \quad (b = 1,2; j = 1,2 \cdots n) \quad (9)$$

where i was number of iteration. The iteration was finished when the following convergence criterion was gained.

$$\delta = \max_{\substack{b=1,2 \\ j=1,2 \cdots n}} \left| \frac{t_{bj}^{i+1} - t_{bj}^i}{t_{bj}^i} \right| \leq 1.0\% \quad (10)$$

Otherwise, the iteration will be continued using Eqs. (1)-(10). Then optimized material distribution in Fig. 1(d) was derived. Finally, brace configuration in Fig. 1(e) was established using discrete method presented in Zhou and Li (2005). Moreover, modified structure in Fig. 1(f) was proposed by merging two adjacent nodes for manufactured simplification.

2.2 Comprehensive seismic performance analysis

Comprehensive seismic performance analysis was studied using static nonlinear analysis (or pushover) and incremental dynamic analysis (or IDA). Pushover was used to obtain structural strength, stiffness and ductility. In addition, IDA was used to assess collapse and demolition fragility, and dynamic instability was taken as collapse state in Vamvatsikos and Cornell (2002).

In order to realize IDA and quantify structural seismic fragility, a set of ground motion records was necessary. Record selection criteria were presented in FEMA P695 (2009), e.g. earthquake magnitude of ground motion record exceeded 6.5 and limit of peak ground acceleration (*PGA*) was greater than 0.2 g. Furthermore, far-field record set includes twenty-two records from 14 earthquake events was recommended for stiff soil sites in FEMA P695 (2009), which has been used in many previous studies.
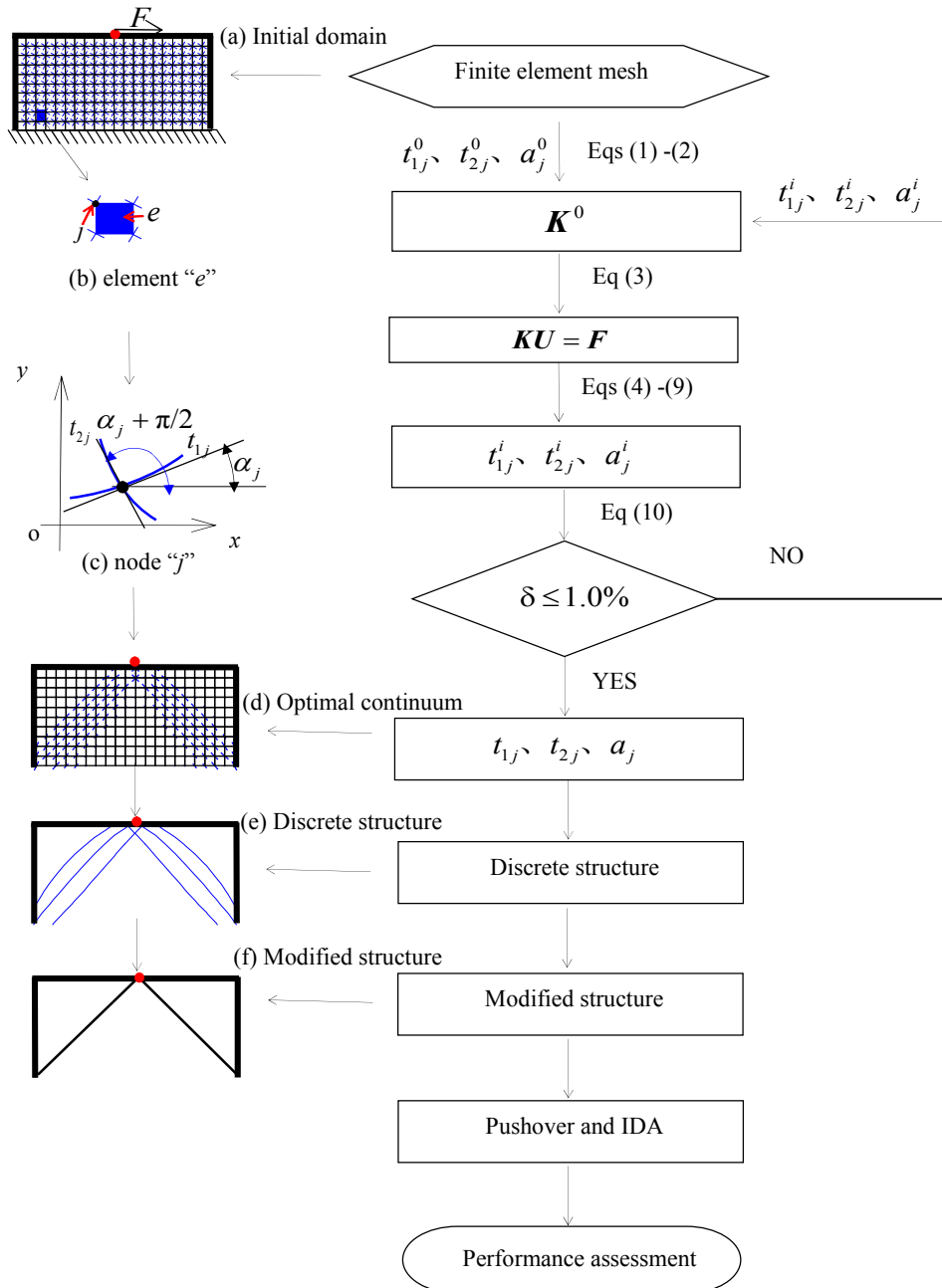
Fig. 1 Seismic performance analysis flowchart of steel-brace RC frame using topology optimization

3. Numerical cases

3.1 Original RC frames

Structure layouts of existing 3-story, 6-story and 9-story RC frames were same as introduced in Fig. 2(a). For simplification, 2D 3-story, 6-story and 9-story frames (hereinafter referred to as low-rise, mid-rise and high-rise frame, respectively) were used in Figs. 2(b)-(d). Aforementioned RC frames were in seismic region of 8 degree protected earthquake intensity in Table 1 according to GB50011 (2016). Site predominant period T_g was 0.40s. The soil site is stiff, and bottom column was rigidly connected to the foundation. Dead and live distributed loads

Table 1 8 degree protected earthquake intensity

Seismic level	Minor earthquake	Moderate earthquake	Rare earthquake
Peak ground acceleration(g)	0.07	0.20	0.40
Exceedance probability in 50 years	63.2%	10.0%	2.0%

were 3.5 kN/m^2 and 2.0 kN/m^2 on the floors respectively,and linear load of infilled wall was 8.0 kN/m on beams in GB50009 (2012). Therefore, representative value of gravity load based on load combinations was 30.5 kN/m (3.5×1.0×5.0+2.0×0.5×5.0+8.0=30.5) on beams in GB50011 (2016). Moreover, the mass was 21.2 t, which was concentrated at each beam-column connections. Uniaxial material Concrete01 or Steel01 could be derived in OpenSEES (2013).
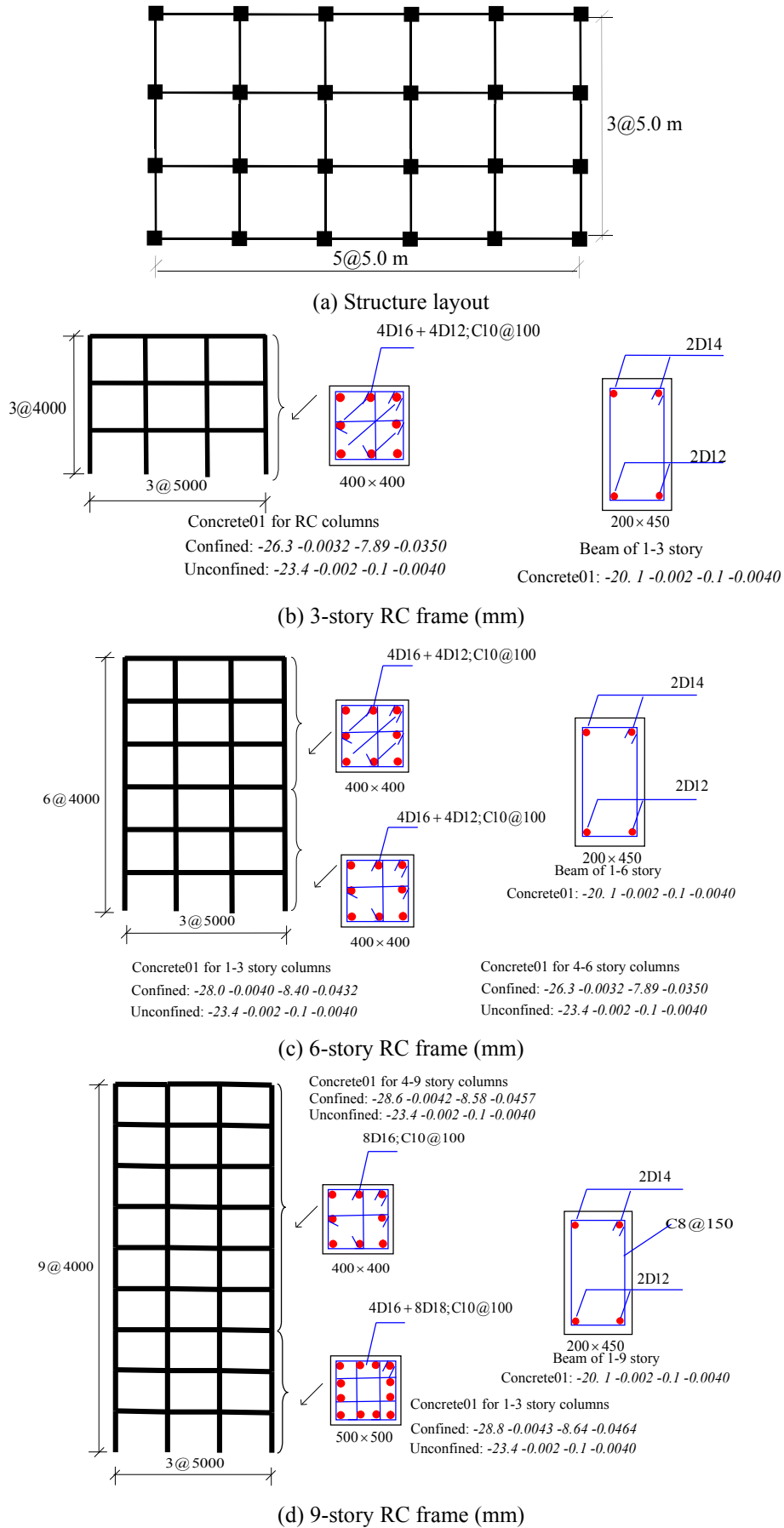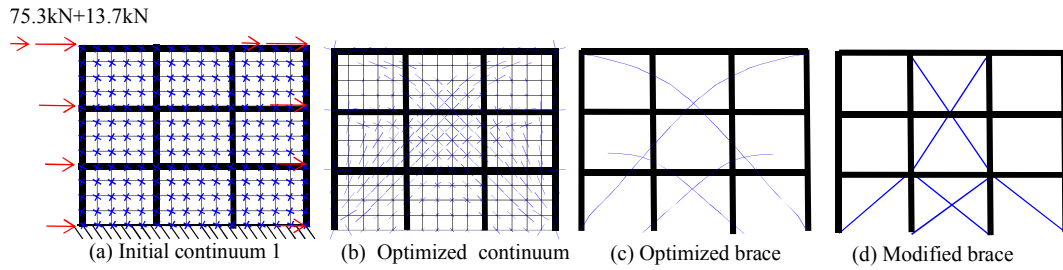
(a) Structure layout

3@5.0 m

5@5.0 m

4D16 + 4D12;C10@100

2D14

2D12

400 × 400

200 × 450

3@4000

3@5000

Concrete01 for RC columns
Confined: *-26.3 -0.0032 -7.89 -0.0350*
Unconfined: *-23.4 -0.002 -0.1 -0.0040*

Beam of 1-3 story
Concrete01: *-20. 1 -0.002 -0.1 -0.0040*

(b) 3-story RC frame (mm)

4D16 + 4D12;C10@100

2D14

2D12

400 × 400

4D16 + 4D12;C10@100

200 × 450
Beam of 1-6 story
Concrete01: *-20. 1 -0.002 -0.1 -0.0040*

400 × 400

6@4000

3@5000

Concrete01 for 1-3 story columns
Confined: *-28.0 -0.0040 -8.40 -0.0432*
Unconfined: *-23.4 -0.002 -0.1 -0.0040*

Concrete01 for 4-6 story columns
Confined: *-26.3 -0.0032 -7.89 -0.0350*
Unconfined: *-23.4 -0.002 -0.1 -0.0040*

(c) 6-story RC frame (mm)

Concrete01 for 4-9 story columns
Confined: *-28.6 -0.0042 -8.58 -0.0457*
Unconfined: *-23.4 -0.002 -0.1 -0.0040*

8D16;C10@100

2D14

C8@150

2D12

400 × 400

4D16 + 8D18;C10@100

200 × 450
Beam of 1-9 story
Concrete01: *-20. 1 -0.002 -0.1 -0.0040*

500 × 500

Concrete01 for 1-3 story columns
Confined: *-28.8 -0.0043 -8.64 -0.0464*
Unconfined: *-23.4 -0.002 -0.1 -0.0040*

9@4000

3@5000

(d) 9-story RC frame (mm)
Fig. 2 Original RC frames (mm)

75.3kN+13.7kN

| (a) Initial continuum 1 | (b) Optimized continuum | (c) Optimized brace | (d) Modified brace |

Fig. 3 Optimized bracing system of low-rise frame

41.6kN+27.5kN

(a) Initial continuum   (b) Optimized continuum   (c) Optimized brace   (d) Modified brace
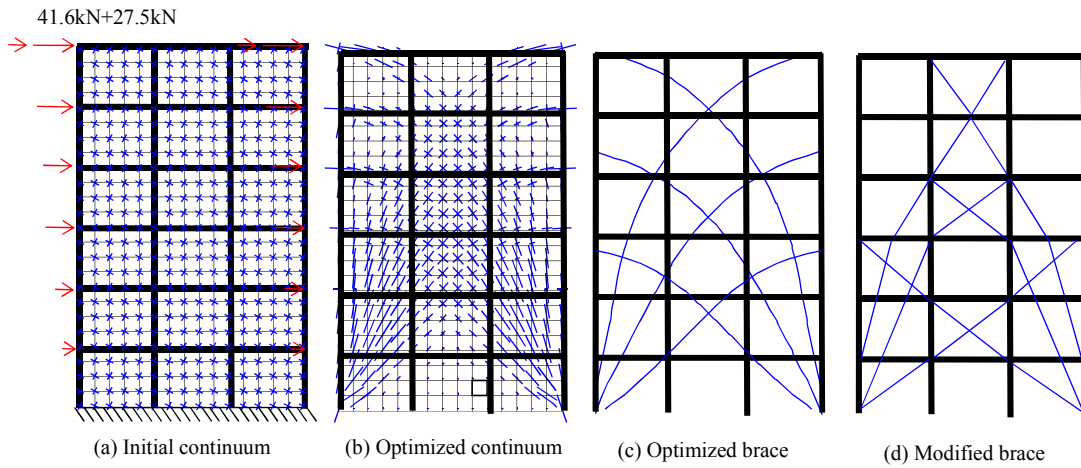
Fig. 4 Optimized bracing system of mid-rise frame

36.8kN+49.4kN

(a) Initial continuum   (b) Optimized continuum   (c) Optimized brace   (d) Modified brace
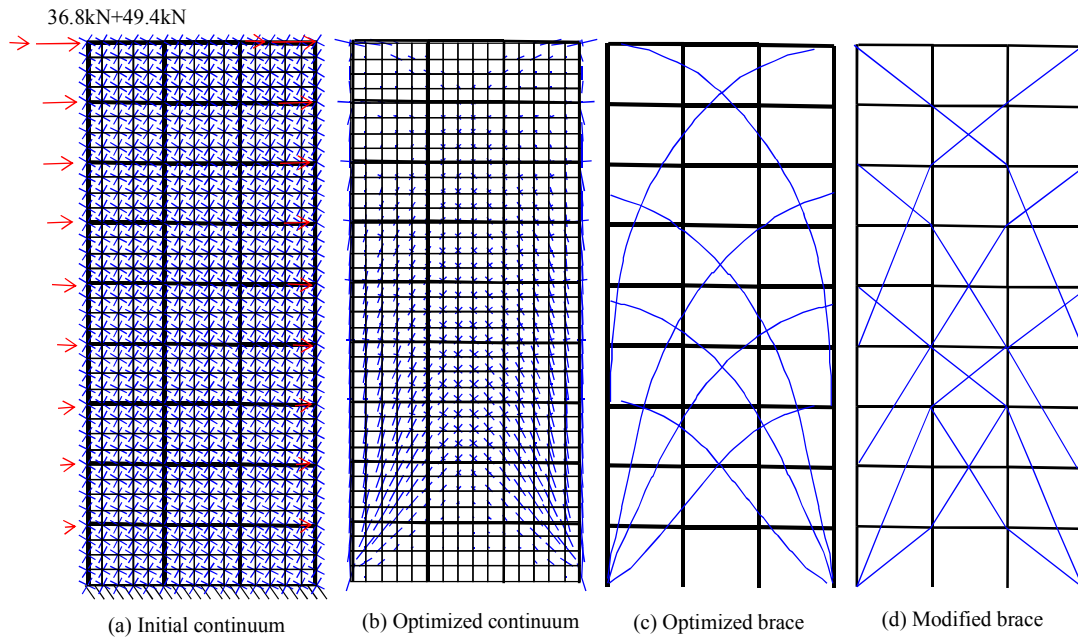
Fig. 5 Optimized bracing system of high-rise frame

3.2 Optimized brace systems

Finite element mesh with 180 rectangular elements was used to divide the low-rise original frame (or OF) in Fig. 3(a). Then initial truss-like continuum was derived by initializing densities and directions of truss-like members in

Fig. 3(a), and initial stiffness matrix could be established using Eqs. (1)-(2). E was 200 Gpa and σ_y was 235 Mpa.

The fundamental periods of low-rise, mid-rise and high-rise frames were 0.92 s, 1.86 s and 2.52 s accordingly. Relevant total seismic action (F_0) under minor earthquake was calculated using bottom shear method in GB50011
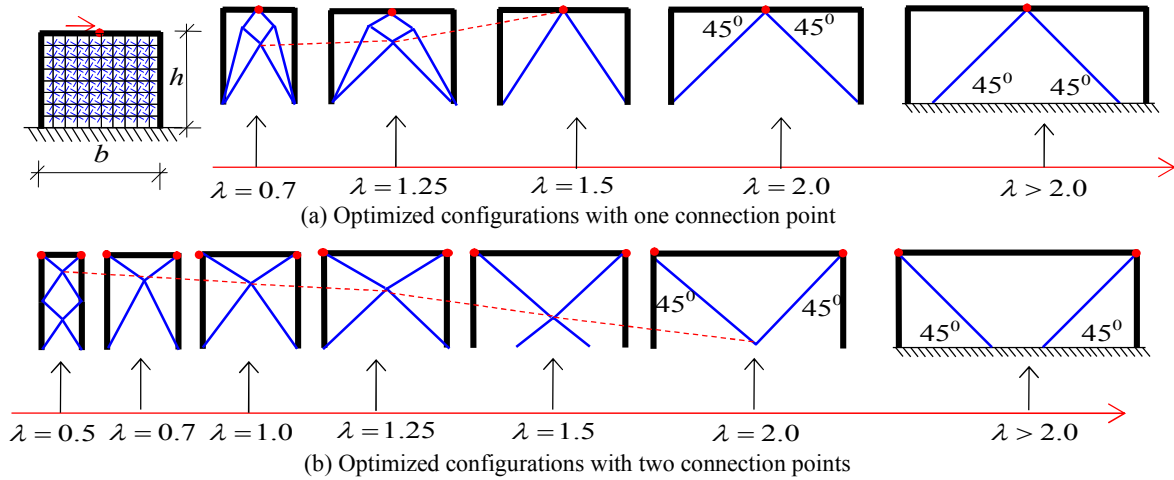
(a) Optimized configurations with one connection point

(b) Optimized configurations with two connection points

Fig. 6 Optimized configurations of different constraints

Table 2 Relevant seismic action using bottom shear method

Frame type	low-rise	mid-rise	high-rise
Fundamental period (s)	0.92	1.86	2.52
T_g(s)	0.40	0.40	0.40
Seismic influence coefficient	0.076	0.040	0.036
Equivalent gravity load(kN)	2162.4	4324.8	6487.5
Total seismic action F_0(kN)	164.3	173.0	233.5
ΔF (kN)	13.7	27.5	49.4

(2016), and additional force ΔF represented higher mode effects in Table 2. Lateral seismic action pattern was determined as follows,

$$F_i = \frac{m_i H_i}{\sum\limits_{j=1}^{n} m_j H_j}(F_0 - \Delta F) \qquad (11)$$

Where m_i and F_i were mass and seismic action of story i. H_i was height between the base and story i. Thus, seismic action of low-rise frame was demonstrated in Fig. 3(a). Furthermore, base was fixed fully. Then optimized material distribution in Fig. 3(b) was obtained. The optimal bracing system in Fig. 3(c) was proposed using the discrete method in Zhou and Li (2005). In order to avoid cutting columns, modified bracing system in Fig. 3(d) was proposed by combining two adjacent nodes with beam-column connections.

Moreover, bracing systems of the mid-rise and high-rise RC frames were derived in Figs. 4-5 likewise. However, the brace systems in Figs. 3-5 were established, while not considering some actual limitations, such as infilled wall and curtain wall. Therefore, it was not agree with the practical conditions sometimes. Generally, braced frame was more available to utilize in each substructure. Bracing system of substructure was related to parameter λ in Qiao *et al.* (2016).

$$\lambda = b / h \qquad (12)$$

Where b was span and h was story height. Therefore, optimized configurations of different constraints were derived under different λ using topology optimization in Fig. 6(a), in which only one connection point in the beam span. Moreover, optimized configurations with two connection points were also demonstrated in Fig. 6(b).

3.3 Model in OpenSEES

Low-rise, mid-rise and high-rise bracing systems of topology optimization (TPB) based on entire structure were presented in Figs. 7(a)-(c). Moreover, inverted V-brace (or IVB), X-brace (or XB) and single-bar brace (or SBB) were also used, which were presented in Figs. 7(a)-(c), respectively.

Low-rise, mid-rise and high-rise frames were introduced above in Fig. 2. Concrete01 was used to depict concrete material in Fig. 8(a), and detailed parameter settings were presented in Fig. 2. Steel01 was used to represent steel and brace material constitutive without buckling in Fig. 8(b). Material constitutive of buckling brace was introduced in Fig. 8(c) based on Papadrakakis (1983). Brace information was displayed in Table 3. f_y was denote yielding stress, and f_{cr} was Euler critical buckling stress.

$$f_{cr} = \pi^2 EI \big/ Al^2 \qquad (13)$$

Where E and A were elasticity modulus and cross-sectional area. I was moment of inertia and l was effective length.

Moreover, beam and column elements were simulated using nonlinearBeamColumn with fiber section. Beam-column connection was assumed as rigid. In addition, experiments of RC frame in Duong *et al.* (2007) and column in Tanaka *et al.* (1990) were simulated in Figs. 8(d)-(e).
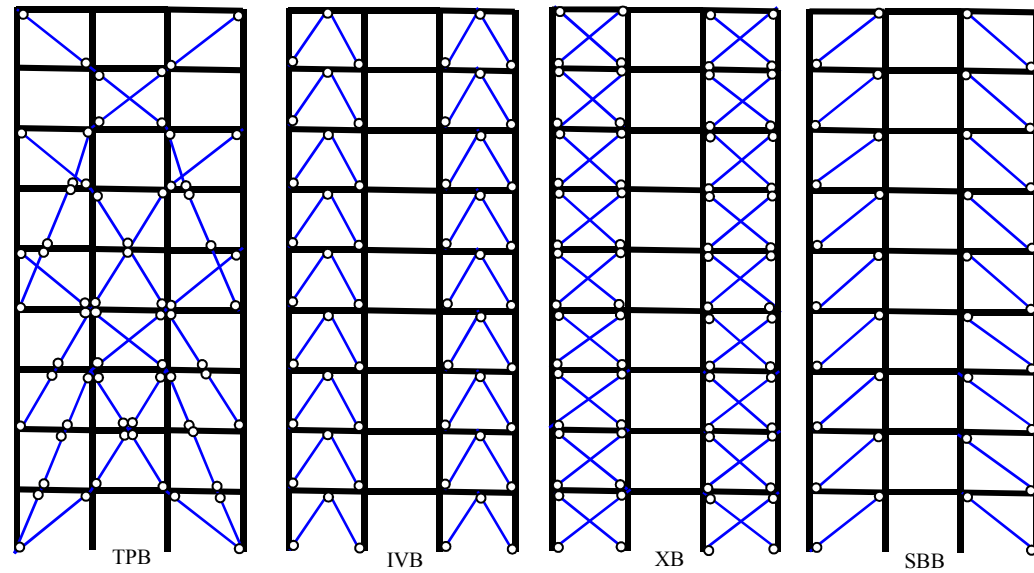
Fundamental periods of structures were derived in Table 4 with brace buckling or not.
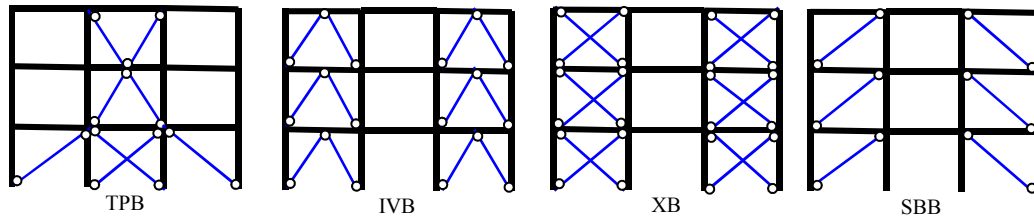
(a) Bracing systems of low-rise frame
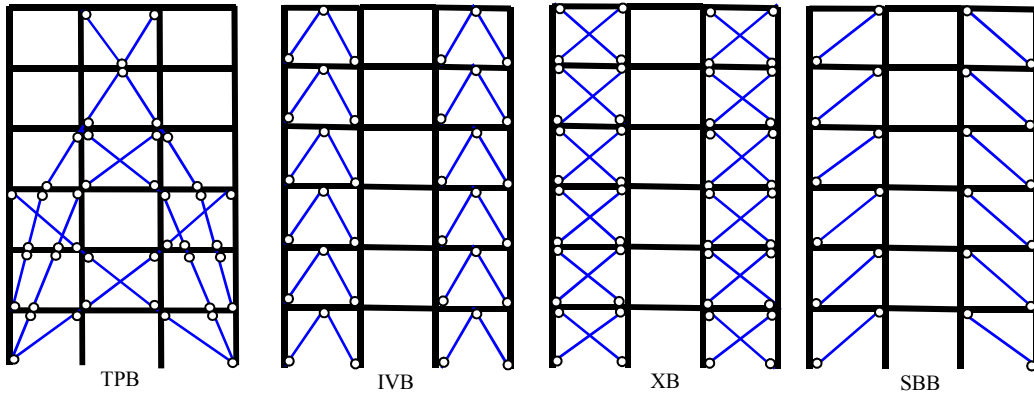
(b) Bracing systems of mid-rise frame

(c) Bracing systems of high-rise frame

Fig. 7 Bracing systems of low-, mid- and high-rise frames

Table 3 Braces of low-/ mid-/ high-rise frames

Brace configuration	TPB	IVB	XB	SBB
Sectional area A(mm^2)	345/377/539	272/407/543	200/300/400	400/600/800
Box section(mm)	50-50-1.7/1.9/2.7	50-50-1.4/2.0/2.7	50-50-1.0/1.5/2.0	50-50-2.0/3.0/4.0
Total length(m)	44.5/122.3/171.5	56.6/113.2/169.8	76.8/153.7/230.6	38.4/76.8/115.3
Total volume(m^3)	0.0153/0.0462/0.0922			
Element type	Truss			
Material constitutive	Steel01, Hysteretic			
Component length l(m)	4.7, 6.4/ 4.3, 4.7, 6.4/ 4.3, 4.7, 6.4	4.7/4.7/4.7	6.4/6.4/6.4	6.4/6.4/6.4
Critical buckling stress(MPa)	34.3, 18.6/ 40.2, 34.0, 18.4/ 38.3, 32.3, 17.5	35.0/33.6/32.3	19.4/18.8/18.3	18.2/17.1/16.2

Uniaxial Material Concrete01 $matTag $fpc $epsc0 $fpcu $epsU
$matTag: material tag $fpc $epsc0 $fpcu $epsU
$fpc: concrete compressive strength
$epsc0: concrete strain at maximum strength
$fpcu: concrete crushing strength
$epsU: concrete strain at crushing strength

(a) Concrete01 for beams and columns

Steel01 for RC elements:
400 200000 0.01
Steel01 for braces without buckling:
235 200000 0.00

(b) Steel01 for steel

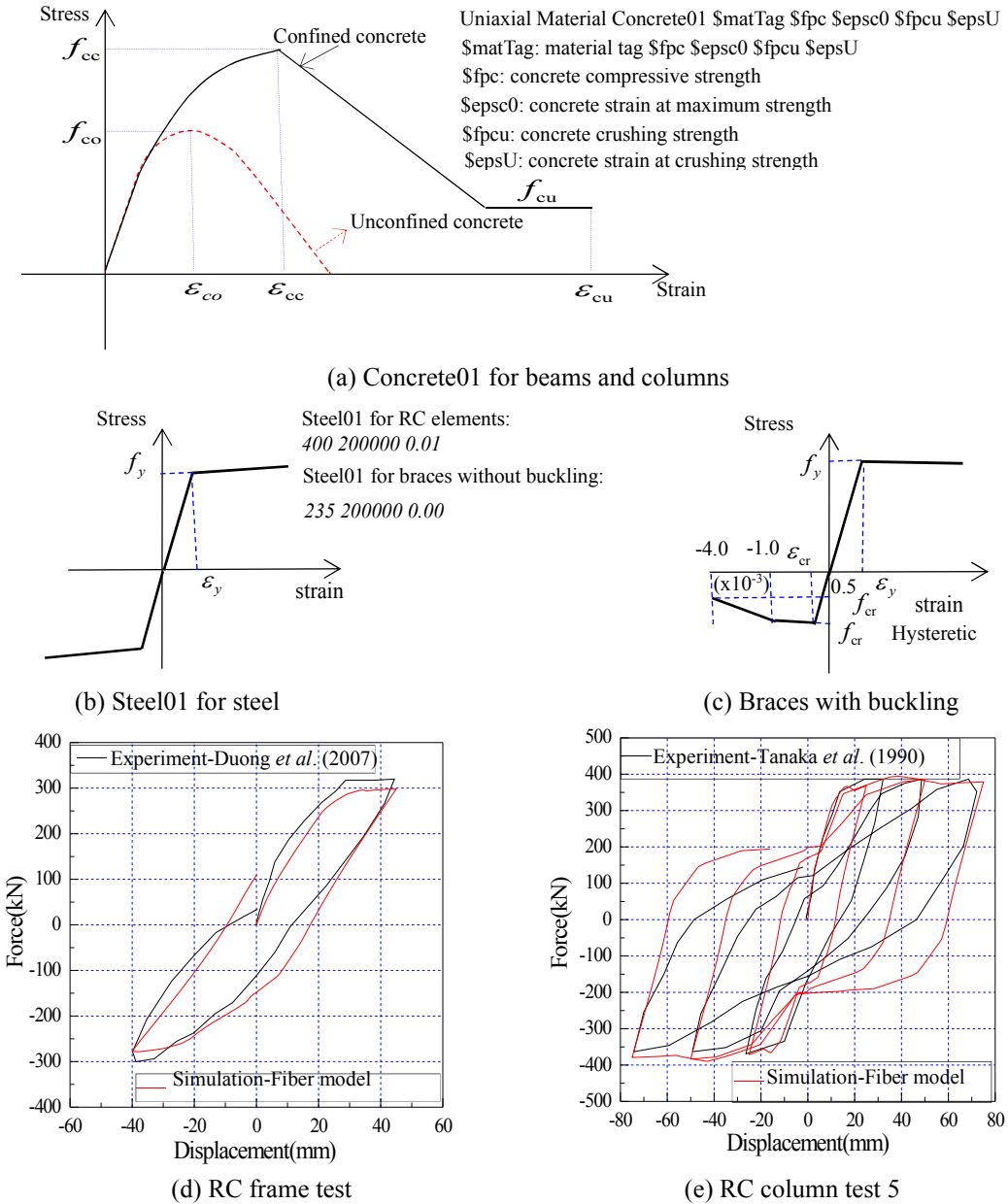(c) Braces with buckling

(d) RC frame test

(e) RC column test 5

Fig. 8 Constitutive relation and fiber model

Table 4 Fundamental periods of low-/ mid-/ high-rise frames

No Buckling (3/6/9-storey)				
Types	OF	TPB	IVB	XB	SBB
T_1 (s)	0.94/1.86/2.52	0.70/1.25/1.62	0.72/1.30/1.74	0.70/1.26/1.70	0.70/1.26/1.70
Reduction (%)	--	25.5/32.9/35.6	23.4/30.0/30.1	25.5/32.2/32.6	25.5/32.2/32.6
Buckling(9-storey)				
Types	OF	TPB	IVB	XB	SBB
T_1 (s)	2.52	1.62	1.74	1.70	1.70
Reduction (%)	--	35.6	30.1	32.6	32.6

(a) Low-rise (no buckling)

(b) Low-rise (buckling)

(c) Mid-rise (no buckling)

(d) Mid-rise (buckling)

(e) High-rise (no buckling)
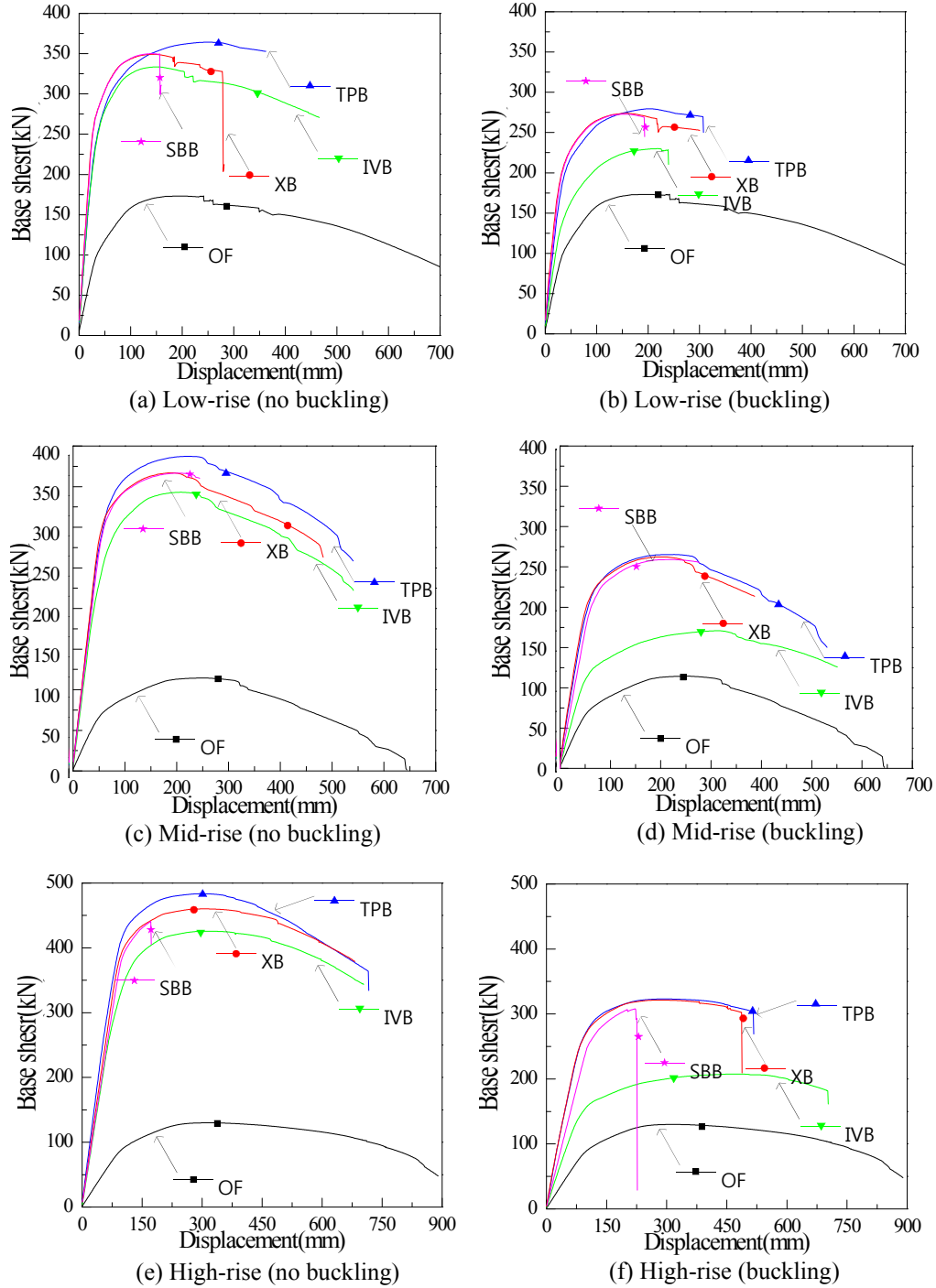
(f) High-rise (buckling)

Fig. 9 Pushover curves

3.4 Static nonlinear analysis

Lateral load pattern of inverted triangular was used in pushover process. Pushover curves of low-rise frames without brace buckling were demonstrated in Fig. 9(a), while considering brace buckling in Fig. 9(b). Similarly, pushover curves of mid-rise and high-rise frames were presented in Figs. 9(c)- (d) and Figs. 9(e)- (f).

With the help of equivalent elasto-plastic energy method, some parameters could be obtained from Fig. 9(a) without brace buckling in Table 5, e.g. the maximum base shear F_{max}, yielding base shear F_y, ultimate roof

displacement u_u and yielding roof displacement u_y of low-rise structure. Mid-rise and high-rise structures were also obtained from Fig. 9(c) and Fig. 9(e), respectively. Ultimate base shear F_u was calculated as follows.

$$F_u = 0.85 F_{max} \quad (14)$$

Ductility factor β_u was also derived in Table 5.

$$\beta_u = u_u / u_y \quad (15)$$

Similarly, the same parameters with brace buckling were established in Table 6.

Table 5 Maximum base shear and ductility factors without buckling

Low-rise frame					
Configurations	F_u (kN)	F_y (kN)	u_u (mm)	u_y (mm)	Ductility factor
OF	173.5	147.1	420.3	82.5	5.09
TPB	364.2	311.9	362.5	71.5	5.07
IVB	333.6	286.3	419.8	54.8	7.68
XB	349.2	298.6	278.7	46.6	5.97
SBB	349.9	300.4	159.5	47.8	3.33
Mid-rise frame					
Configurations	F_u (kN)	F_y (kN)	u_u (mm)	u_y (mm)	Ductility factor
OF	114.5	95.5	354.3	118.7	2.98
TPB	387.3	345.0	418.7	82.1	5.10
IVB	343.0	299.7	397.6	87.1	4.56
XB	366.9	326.6	384.0	74.3	5.17
SBB	366.6	328.4	244.5	78.8	3.10
High-rise frame					
Configurations	F_u (kN)	F_y (kN)	u_u (mm)	u_y (mm)	Ductility factor
OF	124.7	108.3	550.6	159.6	3.45
TPB	483.6	436.8	593.7	116.8	5.08
IVB	425.7	380.1	653.8	131.5	4.97
XB	460.2	416.1	649.4	121.3	5.35
SBB	440.6	404.3	172.8	115.8	1.49

Table 6 Maximum base shear and ductility factors with buckling

Low-rise frame					
Configurations	F_u (kN)	F_y (kN)	u_u (mm)	u_y (mm)	Ductility factor
OF	173.5	147.1	420.3	82.5	5.09
TPB	279.5	235.9	307.5	68.9	4.46
IVB	229.9	192.2	239.7	80.5	2.98
XB	273.8	232.6	300.5	52.4	4.19
SBB	272.8	233.0	193.4	54.1	3.58
Mid-rise frame					
Configurations	F_u (kN)	F_y (kN)	u_u (mm)	u_y (mm)	Ductility factor
OF	114.5	95.5	354.3	118.7	2.98
TPB	265.4	233.0	382.4	82.1	4.66
IVB	170.7	143.2	470.1	115.0	4.09
XB	262.4	230.2	351.6	77.4	4.54
SBB	259.1	230.3	259.1	89.7	3.08
High-rise frame					
Configurations	F_u (kN)	F_y (kN)	u_u (mm)	u_y (mm)	Ductility factor
OF	124.7	108.3	550.6	159.6	3.45
TPB	323.3	289.4	516.8	118.1	4.38
IVB	207.6	177.7	702.3	162.4	4.32
XB	321.3	285.1	437.3	116.8	4.17
SBB	307.9	278.5	225.9	134.6	1.67

3.5 Dynamic time history analysis

Soil site was stiff, therefore, far-field record set includes twenty-two records (or E1~E22) was used in FEMA P695 (2009). Rayleigh damping was 5%. *PGA* was proposed as seismic intensity parameter during dynamic time history analysis in GB50011 (2016), and *PGA* could also be considered as seismic intensity parameter in IDA according to Vamvatsikos and Cornell (2002). Hence, *PGA* was taken as seismic intensity parameter in this study.

IDAs of different 9-story structures were simulated in OpenSEES (2013). Thus, IDA curves of OF were derived in Fig. 10(a) without brace buckling by recording maximum inter-story drift ratio (*MIDR*) of each time-history analysis. And IDA curves of TPB, IVB, XB and SBB were obtained in Figs. 10(b)-(e), respectively. Dynamic instability was

(a) IDA curves of OF

(b) IDA curves of TPB

(c) IDA curves of IVB

(d) IDA curves of XB

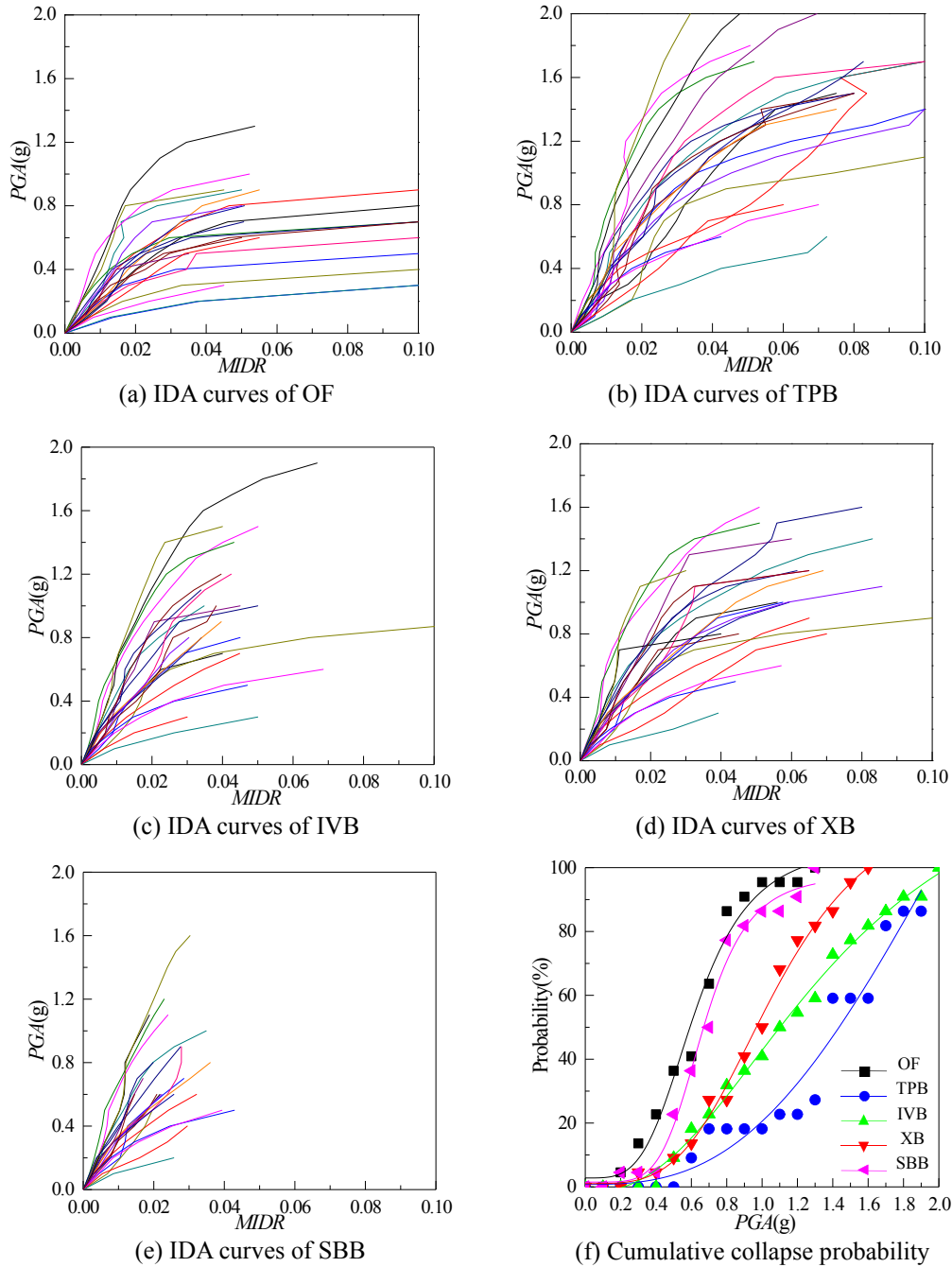(e) IDA curves of SBB

(f) Cumulative collapse probability

Fig. 10 IDA curves of 9-story frame without buckling

taken as collapse state in Vamvatsikos and Cornell (2002). Therefore, cumulative collapse probability curves as well as logarithmic curve fitting were shown in Fig. 10(f).

Simultaneously, maximum residual inter-story drift ratios (*RIDR*) of five aforementioned structures were shown in Figs. 11(a)-(e). Many RC structures have to be demolished due to excessive residual inter-story drift based on past-earthquakes in Ramirez and Miranda (2012). The demolition probabilities were approximate 10%, 50% and 85% if the *RIDR*s were 1.0%, 1.5% and 2.0% accordingly in Ramirez and Miranda (2012). Moreover, cumulative demolition probability (including demolition probability and collapse probability) curves of different structures were gained in Figs. 11(f)-(h) when *RIDR*s of 1.0%, 1.5% and

2.0% were taken as demolition limit, respectively.

Similarly, cumulative collapse probability curves and cumulative demolition probability curves were derived in Figs. 12(a)-(d) when brace buckling was considered. In addition, *PGAs* in terms of medians of cumulative collapse probability curves and cumulative demolition probability curves were obtained in Table 7 with brace buckling or not. Relevant collapse margin ratio (*CMR*) was acquired as follows in Table 7.

$$CMR = PGA_{50\%} \, / \, MCE \qquad (16)$$

Where *MCE* was 0.40 g under rare earthquake, and *PGA*$_{50\%}$ corresponds to the median of cumulative collapse probability curve.

(a) IDA curves of OF

(b) IDA curves of TPB

(c) IDA curves of IVB

(d) IDA curves of XB

(e) IDA curves of SBB

(f) Cumulative demolition probability
(*RIDR* of demolition limit=1.0%)

(g) Cumulative demolition probability
(*RIDR* of demolition limit=1.5%)

(h) Cumulative demolition probability
(*RIDR* of demolition limit=2.0%)
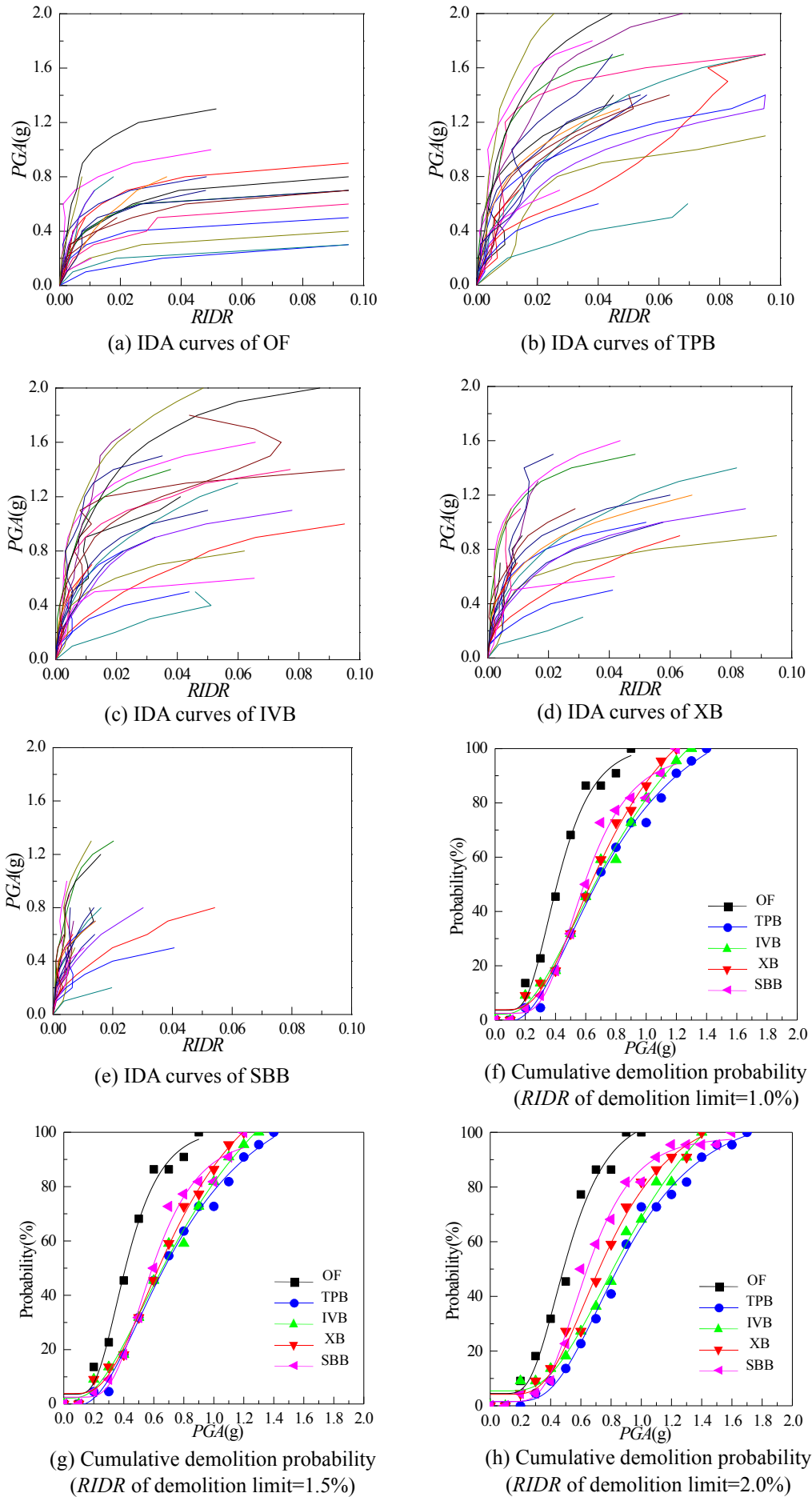
Fig. 11 IDA curves of 9-story frame without buckling (*RIDR*)

(a) Cumulative collapse probability

(b) Cumulative demolition probability
(*RIDR* of demolition limit=1.0%)

(c) Cumulative demolition probability
(*RIDR* of demolition limit=1.5%)

(d) Cumulative demolition probability
(*RIDR* of demolition limit=2.0%)
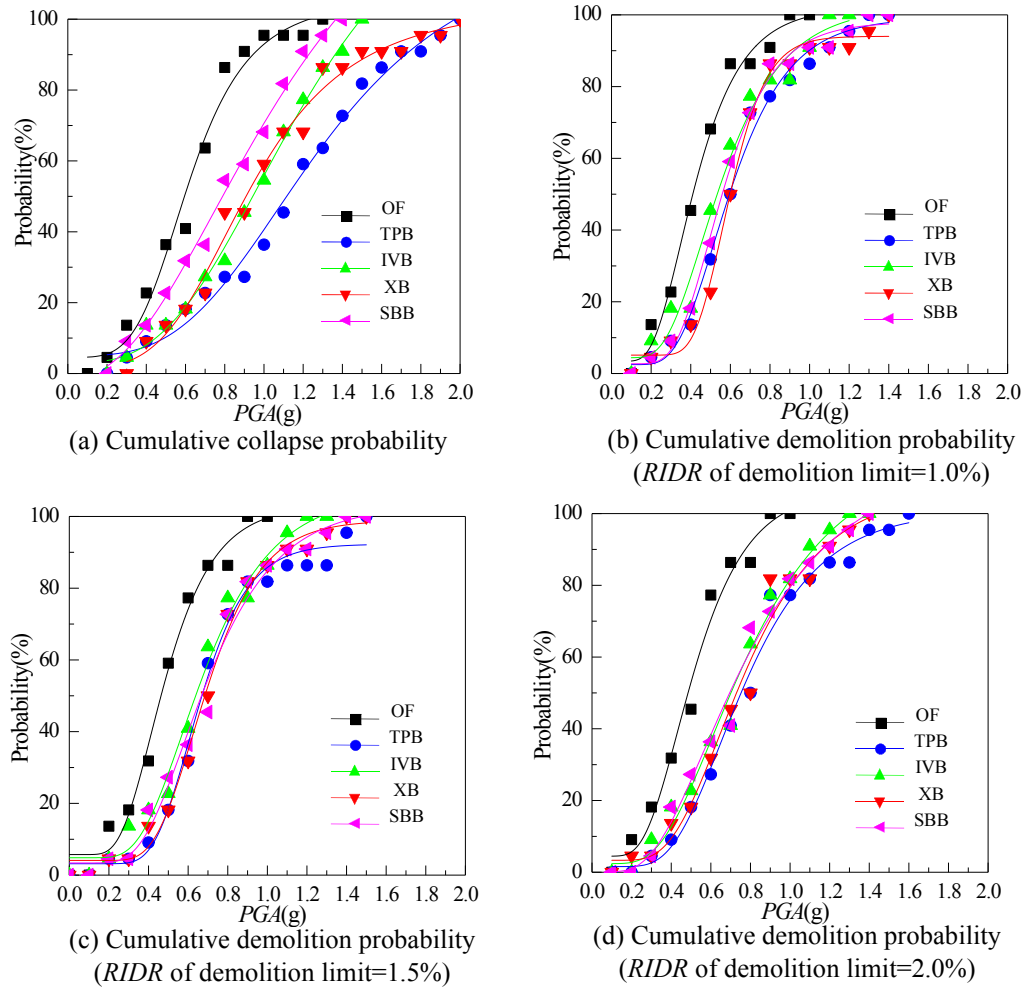
Fig. 12 Cumulative collapse and demolition probability curves of 9-story frame with buckling

Table 7 Collapse resistant capacity and demolition median of high-rise frame

Without buckling				
Configurations	Demolition median			Collapse median (*CMR*)
	RIDR=1.0%	*RIDR*=1.5%	*RIDR*=2.0%	
OF	0.41 g	0.46 g	0.48 g	0.53 g(1.33)
TPB	0.66 g	0.75 g	0.84 g	0.95 g(2.38)
IVB	0.64 g	0.73 g	0.80 g	0.84 g(2.10)
XB	0.62 g	0.67 g	0.71 g	0.76 g(1.90)
SBB	0.59 g	0.63 g	0.64 g	0.65 g(1.63)
With buckling				
Configurations	Demolition median			Collapse median (*CMR*)
	RIDR=1.0%	*RIDR*=1.5%	*RIDR*=2.0%	
OF	0.41 g	0.46 g	0.48 g	0.53 g(1.33)
TPB	0.59 g	0.67 g	0.75 g	0.83 g(2.08)
IVB	0.53 g	0.63 g	0.69 g	0.73 g(1.83)
XB	0.59 g	0.68 g	0.73 g	0.75 g(1.88)
SBB	0.55 g	0.67 g	0.69 g	0.70 g(1.75)

Table 8 Collapse probability and demolition probability of high-rise frame under rare earthquake

Configurations	Without buckling			
	Demolition probability (%)			Collapse probability (%)
	RIDR=1.0%	*RIDR*=1.5%	*RIDR*=2.0%	
OF	22.7	9.1	9.1	22.7
TPB	9.1	4.5	0.0	9.1
IVB	9.1	4.5	4.5	9.1
XB	9.1	4.5	4.5	9.1
SBB	9.1	4.5	0.0	9.1
Configurations	With buckling			
	Demolition probability (%)			Collapse probability (%)
	RIDR=1.0%	*RIDR*=1.5%	*RIDR*=2.0%	
OF	22.7	9.1	9.1	22.7
TPB	9.1	4.5	4.5	4.5
IVB	4.5	4.5	4.5	13.6
XB	0.0	0.0	0.0	13.6
SBB	0.0	0.0	0.0	18.2

4. Results and discussion

4.1 Optimized brace systems

Bracing systems of low-rise, mid-rise and high-rise using truss-like model were presented in Figs. 3-5. Numerical instability problems were settled due not to remove or restrain elements. Bracing systems based on integral structure in Figs. 3-5 were difficult to be used for engineering practice with some constraints, e.g. infilled wall or curtain wall. Thus, optimized configurations of substructure in Fig. 6 were more available to practical conditions. Moreover, optimized configurations were different in Fig. 6(a) and Fig. 6(b) due to different λ and different boundary conditions.

In Fig. 6(a), optimized bracing system approximated IVB when λ exceeds 1.5, however, optimized bracing system was different from IVB once λ not exceeds 1.25. Similarly, the optimized bracing system was more analogous to XB when λ not exceeds 1.25, and optimized bracing system was prone to V-type brace when λ exceeds 1.5 in Fig. 6(b). It could be deduced that XB was more appropriate with λ less than 1.25, while IVB or V-type brace was more applicable when λ exceeds 1.5.

4.2 Seismic performance analysis

In Table 4, fundamental period could be decreased by adding brace. The reductions in TPB, XB and SBB were more effective than IVB in low-rise frames, and the decrease in TPB was more favorable than others. XB, SBB were similar and more available than IVB due to λ was 1.25. That was to say TPB was most favorable to enhance structural stiffness, and XB, SBB were more appropriate than IVB. Moreover, the increases of fundamental period in TPB were 1.00, 1.02 and 1.09 times of XB. It means the increase was enhanced from low-rise to high-rise frame in TPB.

In Table 5, the improvements of strength in TPB, IVB, XB, SBB were 110%, 92%, 101%, 102% of OF in low-rise frames. TPB was most favorable to improve strength in term of topology optimization. XB and SBB were more effective than IVB. The same trend could also be confirmed in mid-rise and high-rise frames.

In Table 6, the strengths of TPB, IVB, XB, SBB with buckling were 77%, 69%, 78%, 78% of the relevant strengths without buckling in low-rise frames, while the strengths were 69%, 50%, 72%, 71% in mid-rise frame, and 67%, 49%, 70%, 70% in high-rise frames, respectively. The results indicate that brace buckling could decrease strength compared with no buckling condition, and the decrease was most unfavorable in IVB.

The enhancements of ductility factor in TPB, IVB, XB, SBB were 0%, 51%, 17%, -35% than OF in low-rise frames, and 71%, 53%, 73%, 4% in mid-rise frame, as well as 47%, 44%, 55%, -57% in high-rise frame when buckling was neglected. It shows that the improvements of ductility factor in XB were furthermore than SBB due to more structure members, though XB and SBB were similar in structural stiffness and strength. Moreover, the ductility factor could be improved by adding appropriate brace system. The ductility factors of TPB, IVB and XB without buckling were 1.14, 2.58 and 1.42 times of brace buckling in low-rise frames. It manifests that the buckling could reduce the increase amplitude in ductility factor. The similar trend can also found in mid-rise and high-rise frames.

In conclusion, TPB was most favorable to improve structural stiffness and strength in term of topology optimization of entire structure, especially in mid-rise and high-rise frames. And XB based on optimized configuration of substructure was also beneficial in enhancing structural stiffness and strength. In addition, the increase amplitude of structural stiffness and strength could be weakened due to brace buckling, and IVB with brace buckling was most disadvantageous.

4.3 Seismic fragility analysis

In Table 7, *CMR*s of TPB, IVB, XB, SBB without brace buckling were 1.79, 1.58, 1.43, 1.23 times of OF, while TPB, IVB, XB, SBB with brace buckling were 1.56, 1.38, 1.41, 1.32 times. It indicates collapse resistant capacity could be increased using steel brace, and TPB was most effective to improve the collapse resistant capacity. Moreover, brace buckling could reduce collapse resistant capacity in TPB, IVB and XB.

In Table 7, the medians of accumulated demolition probability without buckling in TPB, IVB, XB, SBB enhance 63%, 59%, 46%, 37% when *RIDR* of demolition limit was 1.5%. While the improvements were 46%, 37%, 48%, 46% once buckling was considered. It could be gleamed that the medians of accumulated demolition probability were increased by adding brace, and the improvement was reduced on account of the brace buckling, especially in TPB, IVB.

In Table 8, the collapse probabilities without buckling in TPB, IVB, XB, SBB decrease 60%, 60%, 60%, 60%, as well as the collapse probabilities with buckling reduce 80%, 40%, 40%, 20% under rare earthquake. The demolition probabilities without buckling in TPB, IVB, XB, SBB decrease 50%, 50%, 50%, 50%, and 50%, 50%, 100%, 100% with buckling when *RIDR* of demolition limit was 1.5%. In addition, the accumulated demolition probability(including collapse probability and demolition probability) of OF, TPB, IVB, XB, SBB were 31.8%, 9.1%, 13.6%, 13.6%, 9.1% and 31.8%, 9.1%, 18.2%, 13.6%, 18.2% when the buckling was neglected or not. It could be concluded that collapse probability and accumulated demolition probability were reduced by adding steel brace; hence the reparability probability of post-earthquake could be improved effectively. The reductions of accumulated demolition probability were weakened on account of the brace buckling. Moreover, TPB was most advantageous to mitigate collapse probability and accumulated demolition probability.

5. Conclusions

Seismic performance analysis of steel-brace RC frame in highly seismic region was studied in this paper. Bracing systems of low-rise, mid-rise and high-rise RC frame were established in topology optimization based on truss-like model. Moreover, seismic performance of OF, TPB, IVB, XB, SBB configurations were evaluated and compared using pushover and IDA. The results of this study could be concluded as follows.
• It is feasible to establish bracing systems of low-rise, mid-rise and high-rise RC frame using topology optimization in highly seismic region. In addition, TPB based on entire structure is most available without some constraints. XB based on substructure could be more favorable with λ less than 1.25, and IVB could be more advisable once λ over 1.5.
• TPB is most effective to enhance structural stiffness and strength, especially in mid-rise and high-rise frames. Moreover, ductility factor could be improved by adding

reasonable brace system. In addition, increase amplitude of structural stiffness and strength could be weakened due to brace buckling, and IVB with brace buckling is most disadvantageous.
• Collapse resistant capacity could be improved using steel brace, and collapse probability is also reduced. TPB is most advantageous, for which the positive effect could be reduced by brace buckling.
• Accumulated demolition probability of RC frame could be reduced by adding brace, and reparability probability of post-earthquake could be improved effectively.

References

Allahdadian, S. and Boroomand, B. (2016), "Topology optimization of planar frames under seismic loads induced by actual and artificial earthquake records", *Eng. Struct.*, **115**(3), 140-154. https://doi.org/10.1016/j.engstruct.2016.02.022.

Akbari, R., Aboutalebi, M.H. and Maheri, M.R. (2015), "Seismic fragility assessment of steel x-braced and chevron-braced RC frames", *Asian J. Civil Eng.***16**(1), 13-27.

ASCE/SEI 41-13 (2013), *Seismic Evaluation and Retrofit Rehabilitation of Existing Building*, American Society of Civil Engineers; USA.

Della, C.G., D'Aniello, M. and Landolfo, R. (2015), "Field testing of all-steel buckling-restrained braces applied to a damaged reinforced concrete building", *J. Struct. Eng.*, **141**. https://doi.org/10.1061/(ASCE)ST.1943-541X.0001080.

Duong, K.V., Sheikh, S. and Vecchio, F.J. (2007), "Seismic Behavior of Shear-Critical Reinforced Concrete Frame: Experimental Investigation", *ACI Struct. J.*, **140**(3), 304-313.

FEMA P695 (2009), *Quantification of Building Seismic Performance Factors*, Federal Emergency Management Agency, Washington, USA.

GB50009 (2012), *Load Code for the Design of Building Structures*, Architecture Industry Press, Beijing, China.

GB50011 (2016), *Code for Seismic Design of Buildings*, Architecture Industry Press, Beijing, China.

Mander, J.B., Priestley, M.J.N. and Park, R. (1988), "Theoretical stress-strain model for confined concrete", *J. Struct. Eng.*, **114**(8), 1804-1826. https://doi.org/10.1061/(ASCE)0733-9445(1988)114:8(1804)

Opensees. Open system for earthquake engineering simulation. (2013), Berkeley, CA: Pacific Earthquake Engineering Research Center, University of California. http://opensees.-berkeley.edu.

Ozcelik, R., Binici, B. and Kurc, O. (2012), "Pseudo dynamic testing of an RC frame retrofitted with chevron braces", *J. Earthq. Eng.*, **16**(4), 515-539. https://doi.org/10.1080/13632469.2011.653297.

Papadrakakis, M. (1983), "Inelastic post-buckling analysis of trusses", *J. Struct. Eng.* **109**(9), 2129-2147. https://doi.org/10.1061/(ASCE)0733-9445(1983)109:9(2129).

Qiao, S.F., Han, X.L., Zhou, K.M. and Ji, J. (2016), "Seismic analysis of steel structure with brace configuration using topology optimization", *Steel Compos. Struct.*, **21**(3), 501-515.

Qiao, S.F., Han, X.L., Zhou, K.M. and Li, W.C. (2017), "Conceptual configuration and seismic performance of high-rise steel braced frame", *Steel Compos. Struct.*, **23**(2), 173-186. https://doi.org/10.12989/scs.2017.23.2.173.

Qiao, S.F. and Zhou, K.M. (2016), "Structural topology optimization under uncertain load based on truss-like material model", *Eng. Mech.*, **33**(3), 252-256.

Ramirez, C.M. and Miranda, E. (2012), "Significance of residual drifts in building earthquake loss estimation", *Earthq. Eng. Struct. Dynam.*, **41**(11), 1477-1493. https://doi.org/10.1002/eqe.2217.

Suksuwan, A. and Spence, S. (2018), "Performance-based multi-hazard topology optimization of wind and seismically excited structural systems", *Eng. Struct.*, **172**, 573-588. https://doi.org/10.1016/j.engstruct.2018.06.039.

Tangaramvong, S. and Tin-Loi, F. (2015), "Optimal performance-based rehabilitation of steel frames using braces", *J. Struct. Eng.*, **141**(10), 1-10(04015015). https://doi.org/10.1061/(ASCE)ST.1943-541X.0001248.

Tanaka, H. and Park, R. (1990), "Effect of Lateral Confining reinforcement on the ductile behavior of reinforced concrete columns", Ph.D. Disseration, University of Canterbury. http://hdl.handle.net/10092/1241.

Vamvatsikos, D. and Cornell, C. (2002), "Incremental dynamic analysis", *Earthq. Eng. Struct. Dynam.*, **31**(3), 491-514. https://doi.org/10.1002/eqe.141.

Zhang, X.J., Maheshwari, S., Ramos, A.S. and Paulino, G.H. (2016), "Macroelement and macropatch approaches to structural topology optimization using the ground structure method", *J. Struct. Eng.*, **142**(11), 1-14(04016090). https://doi.org/10.1061/(ASCE)ST.1943-541X.0001524.

Zhou, K.M. and Li, X. (2005), "Topology optimization of Structures under multiple load cases using a fiber-reinforced composite material model", *Comput. Mech.*, **38**(5), 163-170. https://doi.org/10.1007/s00466-005-0735-9.

Zhu, M., Yang, Yang., Guest, J.K., Shields, M.D. (2017), "Topology optimization for linear stationary stochastic dynamics: applications to frame structures", *Struct. Safety*, **67**, 116-131. https://doi.org/10.1016/j.strusafe.2017.04.004.

PL